STRONG OLIVINE LATTICE PREFERRED ORIENTATION IN BRACHINITE-LIKE ACHONDRITES.

Rachel E. Bernard[1], James M.D. Day[1], and Emily J. Chin[1], [1]Scripps Institution of Oceanography, Sverdrup Hall, 8615 Kennel Way, La Jolla, CA 92037 (Email: rebernard@ucsd.edu).

Introduction: The Antarctic olivine-rich Miller Range (MIL) 090405 and MIL 090206 meteorites are brachinite-like achondrites [1-3]. Debate persists as to whether these classes of meteorites are partial melt residues (primitive) [e.g., 3] or cumulates (differentiated) [e.g., 4]. Analysis of the textures (i.e., foliations, lineations) preserved in brachinite-like achondrites may help to elucidate the origin and formation of these meteorites and their parent asteroids. In particular, olivine lattice preferred orientation (LPO), also referred to as crystallographic preferred orientation (CPO), has the potential to reveal information on igneous and/or deformational processes that formed these textures.

In Earth's mantle, olivine LPO is largely found to result from dislocation, or power law, creep (i.e., solid state deformation). Over the past decades, experiments and modeling efforts have demonstrated that deformation conditions such as temperature, differential stress, water content, and strain geometry may influence the development of olivine LPO "types" [e.g., 5-6] (Fig. 1). As such, six olivine LPO types (commonly referred to as A, B, C, D, E, and AG-type), typically identified through electron backscattered diffraction (EBSD), are often used to infer deformation conditions in terrestrial peridotites. These types refer to the orientation of olivine's three principle axes – [100], [010], [001] – in relation to shear direction, which is determined from a sample's lineation and foliation (thin sections analyzed with EBSD are preferably cut parallel to lineation and perpendicular to foliation).

The formation of these types through extraterrestrial igneous processes has not been studied to our knowledge, although AG-type olivine LPO has been linked to deformation in the presence of melt [7-8]. Studying olivine LPO types in olivine-rich achondrites may inform: (1) whether the lineations and foliations developed in samples resulted from deformation/shock or igneous processes; and (2) whether some LPO types can develop in Earth's mantle at conditions not yet explored experimentally.

We examined olivine LPO types and microstructures preserved in two brachinite-like ungrouped achondrites, MIL 090405 and MIL 090206. A previous study [9] presented the olivine LPO measurements for MIL 090405 and 090206; however, the authors did not connect these crystallographic orientations with the overall sample reference frame, making it impossible to connect the LPO patterns to the six known olivine LPO types.

Method: Analyses were conducted using an Oxford Instruments Symmetry EBSD detector installed on the FEI Apreo FESEM at the University of California San Diego. Large area maps (20 µm step size) of polished thin sections were collected using Oxford Instruments Aztec software and post-processed in the MTEX 5.1.1 toolbox for MATLAB [10]. Contoured pole figures and M- and J-indices – measures of fabric strength [11-12] – were generated for one point-per-grain using a halfwidth of 10 degrees. While the two thin sections contain visible apparent foliations, it is unknown to the authors how these were cut relative to lineation. Therefore, pole figures are presented without rotation, and olivine LPO types are deduced from orientation of crystallographic axes relative to foliation alone.

Brief Sample Description: MIL 090405 is primarily composed of long-axis aligned olivine grains rimmed by finely dispersed grains of metal, sulfide, and chromite [13]. MIL 090206 is similar in terms of mineralogy and

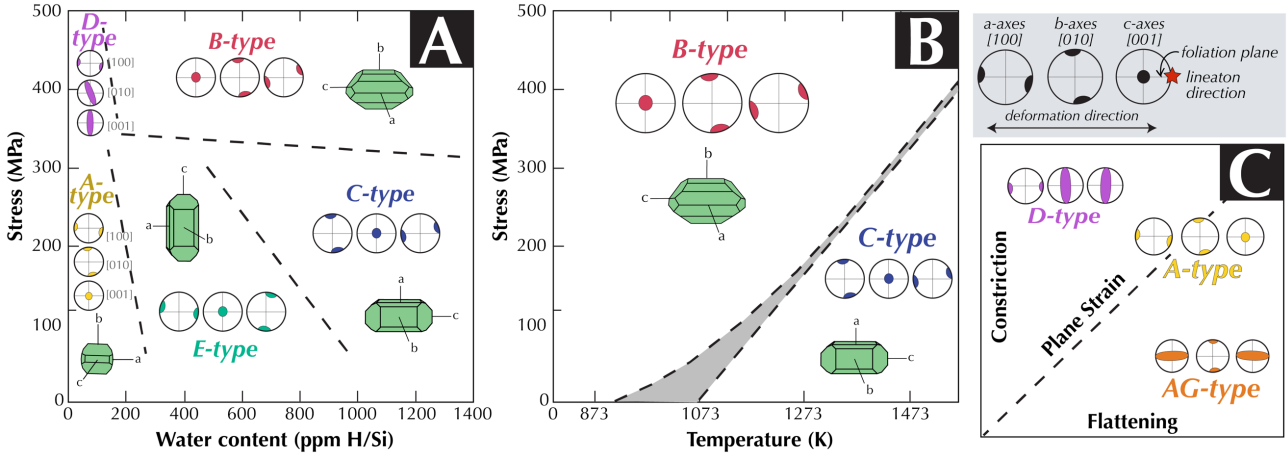

Figure 1: (A-B) Relationships between five olivine LPO types and water, differential stress, and temperature from several experiments summarized in Karato et al. [5]. (C) Relationship between finite strain geometry and three LPO types, based on a figure in Chatzaras et al. [14]. All representative pole figures for each LPO type are based on the reference frame shown in upper right.

microstructural appearance, however the thin section of this sample contains a large (>5 mm) orthopyroxene grain which itself contains tabular olivine grains. According to EBSD phase maps, both samples also contain minor amounts (<5%) of clinopyroxene with grain sizes of ~0.5-1mm in MIL 090405 and <0.1mm in MIL 090206.

Results and Discussion: Both meteorites have strong olivine LPO, apparent from pole figures as well as the relatively uniform coloring of inverse pole figure maps (Fig. 2). Despite having an unknown lineation, we identify likely olivine LPO types based on the pole figure patterns and accompanying maps. Sample MIL 090206 has a strong alignment of olivine [100] (a-axes) and a girdled [010] (b-axes) pattern normal to the apparent foliation plane. The [001] (c-axes) appear weak to randomly oriented. The only established olivine LPO type with girdled b-axes is D-type, associated with activation of the [100]{0kl} slip system. The strong point maxima of the a-axes supports this interpretation. Sample MIL 090405 has a strong orthorhombic olivine LPO. The b-axes are aligned and are subparallel to the foliation plane. The a-axes appear to be aligned normal to that plane, and the c-axes are aligned orthogonal to both of these axes. C-type LPO, associated with activation of the [001](100) slip system, is the only established olivine LPO type where a-axes are aligned normal to foliation and b-axes are aligned within that plane.

Typically, C and D olivine LPO types have been associated with deformation through dislocation creep and/or dislocation-accommodated grain boundary sliding. Deformation experiments have suggested that C-type LPO occurs when water content and/or temperatures are high and D-type LPO occurs when water content is low but differential stress is high (Fig. 1A-B) [e.g., 5]. However, there are documented exceptions where C- and D-type LPO have occurred at other conditions. For example, observations of natural samples have found that D-type LPO may occur at low stress conditions when samples have experienced prolate, or constrictional, deformation (Fig. 1C) [e.g., 14].

Using terrestrial comparisons, the texture of these samples – notably lack of subgrains and internal deformation, along with the aligned, tabular habit of olivine – would suggest a cumulate (rather than shock, or deformational) origin. However, if these samples are instead partial melt residues, the alignment of olivine grains lacking internal deformation may be due to passive alignment in a melt-rich environment. It is confounding as to how an orthorhombic LPO (C-type) could form in such an environment, because girdled [100] and/or [001] axes are instead associated with melt interactions [e.g. 15]. Future work will involve a more detailed study of this sample's microstructures, as understanding the development of this fabric would be of interest to those studying brachinite-like meteorite origins as well as workers interested in olivine LPO, as C-type LPO is exceedingly rare on Earth (<2% of studied samples) [16].

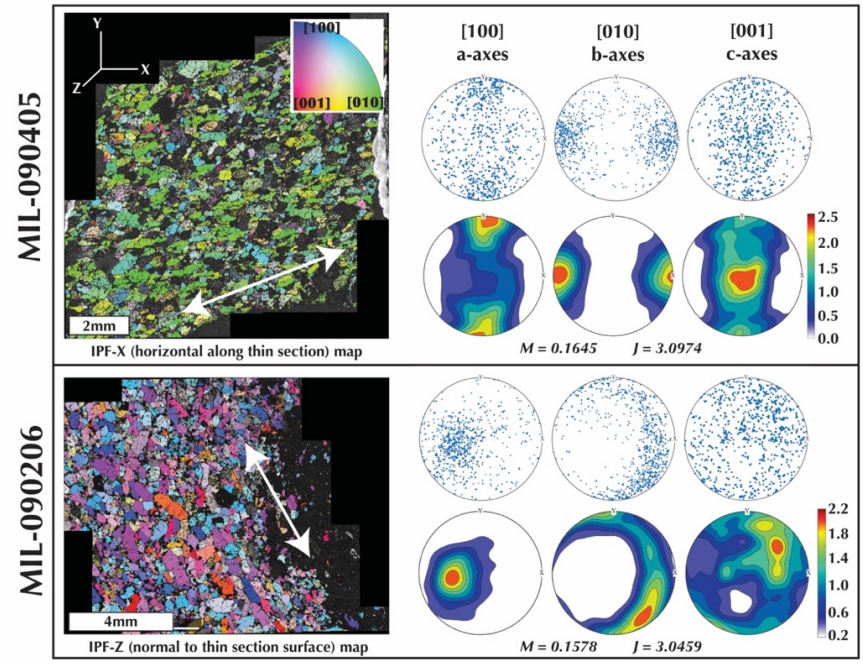

Figure 2: EBSD results from the two samples. (Left) Band contrast maps overlain by inverse pole figure coloring, where olivine grains are colored based on their orientation relative to a specific reference frame direction (X, Y, or Z). The uniformity of colors illustrates the preferential alignment of crystallographic axes. For example, the green coloring in MIL 090405 shows that the olivine [010] axis is aligned in the horizontal (X) direction. White arrows indicate apparent foliation. (Right) Corresponding unrotated pole figures (stereonets). M- and J-indices are shown below contour plots, which are colored by multiples of a uniform distribution and generated for one point-per-grain at a halfwidth of 10 degrees.

References: [1] NASA-JSC (2012) *Antarctic Meteorite Newsletter, 35*, 2. [2] Goodrich C. A. et al. (2012) *AMMS*, Abstract #5272. [3] Day, J. M. D. et al. (2012) *Geochimica et Cosmo. Acta*, *81*, 94-128. [4] Mittlefehldt, D. W. et al. (2003) *Meteoritics & Planet. Sci., 38*, 1601-1625. [5] Karato, S. I. et al. (2008) *Annu. Rev. Earth Planet. Sci.*, *36*, 59-95. [6] A. Tommasi and D. Mainprice (2000) *JGR*, *105,* B4. [7] Qi, C. et al. *GGG*, *19*, 316-336. [8] Holtzmann, B. K. et al. (2003) *Science*, *301*, 1227-1229. [9] Hasegawa, H. et al. (2016) *LPS XLVII*, Abstract #2131. [10] Bachmann, F. et al. (2010) *Solid State Phenomena*, *160*, 63-68. [11] Bunge, H. (1982) *Texture Analysis in Materials Science*, Butterworths, London. [12] Skemer, P. et al. (2005) *Tectonophys, 411,* 157-167. [13] Meteoritical Society (2018) *Meteoritical Bulletin Database*. [14] Chatzaras, V. et al. (2016) *JGR: Solid Earth, 121,* 4895-4922. [15] Chin, E. J. et al. (2016) *GGG, 17,* 2497-2521. [16] Mainprice, D. (2015) *Treatise on Geophysics 2nd ed., vol. 2,* 487-538.